INTERNATIONAL JOURNAL FOR NUMERICAL METHODS IN FLUIDS, VOL. 8, 1469–1490 (1988)

EVALUATION OF FIDAP ON SOME CLASSICAL LAMINAR AND TURBULENT BENCHMARKS

J. L. SOHN

Universities Space Research Association, Fluid Dynamics Branch, NASA/Marshall Space Flight Center, Huntsville, AL *35812, U.S.A*

SUMMARY

Numerical solutions of the Fluid Dynamics Analysis Package (FIDAP) for some laminar and turbulent flow problems, namely (1) two-dimensional laminar flow inside a wall-driven cavity, (2) two-dimensional laminar flow over a backward-facing step and (3) two-dimensional turbulent flow over a backward-facing step, are presented. The consistent integration penalty finite element method is used with Q_2/P_1 (nine-node biquadratic velocity with linear discontinuous pressure) finite elements. Results of FIDAP on the above problems are compared with other numerical solutions and experimental data to evaluate its numerical accuracy. The influence of streamline upwinding is also investigated for all the test cases.

KEY WORDS Finite element method Incompressible fluids Laminar and turbulent flows

INTRODUCTION

Applications of the Galerkin finite element method to incompressible Navier–Stokes equations were introduced in the early 1970s.[1,2] A major difficulty in dealing with incompressible flows is the elimination of spurious pressure modes. Hood and Taylor[3] recognized that the use of equal-order interpolations for both velocity and pressure generates spurious pressure modes, and they obtained better results with a mixed interpolation method which uses the interpolation function for pressure as a polynomial of at least one order lower than that for velocity. However, as numerically proved by Huyakorn *et al.*,[4] the mixed interpolation method does not always provide accurate pressures. For example, a bilinear interpolation for velocity with piecewise constant pressure, which is similar to staggered grids in the finite difference method, works well in some cases but poorly in other cases.

An extensive study of pressure modes in incompressible flows was done by Sani *et al.*[5,6] They explained that the generation of spurious (checker-board) pressure modes is related not only to the selection of interpolation functions for velocity and pressure but also to boundary conditions and element distributions. As a remedy for the checker-board pressure modes, they introduced a Q_2/P_1 element which uses biquadratic (2D) or triquadratic (3D) interpolations for velocity along with linear discontinuous interpolation for pressure. The efficiency of this element was also proved by Oden and Jacquotte.[7]

Sani *et al.*[5] also explained how to combine the idea of the mixed interpolation method and the penalty formulation without selective reduced integrations for the penalty term. The advantage of this consistent integration penalty method over a reduced integration penalty method and its application to a Q_2/P_1 element are demonstrated by Engelman *et al.*,[8] and this combination is a basic algorithm for the treatment of velocity–pressure coupling of incompressible flows in

0271–2091/88/121469–22$11.00

Received 3 December 1987
Revised 4 April 1988

FIDAP.[9] FIDAP also has other choices, such as a mixed interpolation method or a reduced integration penalty method with other types of elements.

Another difficulty in the computation of incompressible flows is the treatment of convection-dominated flows. In this situation the application of the conventional Galerkin finite element method leads to centred differences of the convection terms which cause oscillatory behaviour (wiggles) of velocities or any other flow variables. As mentioned in Gresho and Lee,[10] the obvious way to eliminate wiggles is by mesh refinement in the convection-dominated region. On the other hand, wiggle-free solutions could also be obtained by the use of the 'upwind' finite element scheme. The basic idea of the upwind finite element method was proposed by Christie *et al.*[11] using modified weighting functions. Brooks and Hughes[12] pointed out that this upwinding scheme could generate excessive numerical diffusion perpendicular to the flow direction in multi-dimensional cases. To overcome this shortcoming, they introduced the streamline upwind/Petrov–Galerkin (SUPG) method by modifying the weighting function to add numerical diffusion only in the flow direction. The same idea has also been used by Gresho *et al.*[13] Instead of modifying the weighting function, they defined an additional term, the so-called balancing tensor diffusivity (BTD). FIDAP uses BTD-type streamline upwinding (STU) as an option to eliminate wiggles in convection-dominated flows.[9]

The purpose of this paper is to evalute the numerical accuracy of FIDAP by solving some classical benchmark problems. For this purpose, three well known incompressible laminar and turbulent flow problems are selected, and computational results of FIDAP on these problems are compared with other numerical and experimental data. The influence of numerical diffusion of the streamline upwinding scheme is also investigated.

GOVERNING EQUATIONS

Let Ω denote a bounded flow domain with boundary Γ. The governing equations for a steady, laminar, incompressible flow with isothermal conditions are as follows:

$$\rho U_j \frac{\partial U_i}{\partial x_j} + \frac{\partial P}{\partial x_j} - \mu \frac{\partial^2 U_i}{\partial x_j \partial x_j} = 0 \quad \text{in } \Omega, \tag{1}$$

$$\partial U_i / \partial x_i = 0 \quad \text{in } \Omega \text{ and } \Gamma, \tag{2}$$

with

$$U_i = U_{i0} \quad \text{on } \Gamma_1$$

$$(P\delta_{ij} - \mu \partial U_i / \partial x_j) n_j = t_{0i} \quad \text{on } \Gamma_2.$$

Here $\Gamma_1 \cup \Gamma_2 = \Gamma$ and $\Gamma_1 \cap \Gamma_2 = \varnothing$. In the above equations U_i represents the velocity vector in the x_i-direction, P the pressure, ρ the density, μ the viscosity and t_{0i} the surface traction in the x_i-direction on Γ_2.

In turbulent flow the Reynolds-averaged form of the above equations is

$$\rho \bar{U}_j \frac{\partial \bar{U}_i}{\partial x_j} + \frac{\partial \bar{P}}{\partial x_i} - \left(\mu \frac{\partial^2 \bar{U}_i}{\partial x_j \partial x_j} - \rho \frac{\partial}{\partial x_j} \overline{u_i' u_j'} \right) = 0, \tag{3}$$

$$\partial \bar{U}_i / \partial x_i = 0, \tag{4}$$

with

$$U_i = \bar{U}_i + u_i', \qquad P = \bar{P} + p'$$

and

$$\bar{U}_i = \frac{1}{\Delta t}\int_{t=t}^{t+\Delta t} U_i \mathrm{d}t, \qquad \bar{P} = \frac{1}{\Delta t}\int_{t=t}^{t+\Delta t} P\,\mathrm{d}t, \qquad \overline{u_i' u_j'} = \frac{1}{\Delta t}\int_{t=t}^{t+\Delta t} u_i' u_j' \mathrm{d}t.$$

To close the turbulent momentum equation (3), the standard k–ε turbulence model[14] is used. In this model the Reynolds stress is expressed as

$$-\rho\overline{u_i' u_j'} = \mu_t\left(\frac{\partial \bar{U}_i}{\partial x_j} + \frac{\partial \bar{U}_i}{\partial x_i}\right), \tag{5}$$

where μ_t is a turbulent eddy viscosity defined by

$$\mu_t = \rho C_\mu k^2/\varepsilon. \tag{6}$$

Here, k and ε are the turbulent kinetic energy and its dissipation rate respectively. In the k–ε turbulence model the governing equations for k and ε are

$$\rho\bar{U}_j\frac{\partial k}{\partial x_j} - \frac{\partial}{\partial x_j}\left(\frac{\mu_t}{\sigma_k}\frac{\partial k}{\partial x_j}\right) - \mu_t\left(\frac{\partial \bar{U}_i}{\partial x_j} + \frac{\partial \bar{U}_j}{\partial x_i}\right)\frac{\partial \bar{U}_i}{\partial x_j} + \rho\varepsilon = 0, \tag{7}$$

$$\rho\bar{U}_j\frac{\partial \varepsilon}{\partial x_j} - \frac{\partial}{\partial x_j}\left(\frac{\mu_t}{\sigma_\varepsilon}\frac{\partial \varepsilon}{\partial x_j}\right) - C_1\mu_t\frac{\varepsilon}{k}\left(\frac{\partial \bar{U}_i}{\partial x_j} + \frac{\partial \bar{U}_j}{\partial x_i}\right)\frac{\partial \bar{U}_i}{\partial x_j} + \rho C_2\frac{\varepsilon^2}{k} = 0. \tag{8}$$

Equations (6)–(8) contain empirical constants. In the present study we use the values of these constants recommended by Launder and Spalding.[14]

In turbulent flow it is not convenient to calculate velocities right up to a solid wall because of the existence of a viscous sublayer near the wall where the velocity gradient is very steep. Moreover, the k–ε turbulence model in equations (7) and (8) is not valid near the wall. Thus, generally, the computational domain is not extended to the wall and the wall function is applied to the near-wall region.

As a description of the wall function, the non-dimensional wall distance y^+ is defined as

$$y^+ = U_\tau y/\nu, \tag{9}$$

where ν is the kinematic viscosity and U_τ is a frictional velocity given by

$$U_\tau = \sqrt{\left(\frac{\tau_w}{\rho}\right)} = \sqrt{\left(\nu\frac{\partial U}{\partial y}\right)}.$$

With these definitions, the tangential velocity near the wall is obtained as

$$U = \begin{cases} U_\tau y^+, & 0 < y^+ < 30, \\ (U_\tau/\kappa)\ln(Ey^+), & 30 < y^+ < 100 \end{cases}, \tag{10}$$

where κ is the von Karman constant and E is a roughness parameter. In this study κ and E are set as 0·41 and 9·0 respectively.

NUMERICAL EXAMPLES

Three test cases are selected for the evaluation of the numerical accuracy of FIDAP. They are (1) 2D laminar flow inside a wall-driven cavity, (2) 2D laminar flow over a backward-facing step and (3) 2D turbulent flow over a backward-facing step. The Galerkin formulation of equations in the previous section is discretized by the penalty finite element method with consistent integration.

The selected penalty constant is 10^{-6} for all cases and all Reynolds numbers, and the nine-node quadrilateral finite element with linear discontinuous interpolations for pressure (Q_2/P_1) is used in all test cases. When the streamline upwinding (STU) method is selected, the upwind constant is fixed as 1·0. Computational results of FIDAP are compared with other available CFD solutions and/or experimental data.

2D laminar flow inside a wall-driven cavity

The essential feature of this test case is the prediction of various vortices inside a cavity, as shown in Figure 1. The computational results of the present study are compared with those of Ghia *et al.*[15] who used a multigrid finite difference method for the streamline–vorticity formulations with fine (129 × 129 grid points for $Re < 3200$ and 257 × 257 grid points for $Re > 5000$) but uniform meshes.

In the present study, 40 × 40 elements (81 × 81 grid points) are used with fine meshes near the walls. The non-dimensional characteristic length of the smallest element is 0·00326 at the four corners, and the largest is 0·03074 at the centre of the cavity. The selected Reynolds numbers are 100, 400, 1000, 3200, 5000, 7500 and 10000. To minimize CPU time and to improve initial conditions of the high-Reynolds-number cases, the restart procedure with increments of Reynolds numbers is used. In the case of $Re = 100$, the solution of Stokes flow is chosen as an initial condition. At every selected Reynolds number the successive substitution method is used for the first three iterations for non-linear solutions, and the quasi-Newton method is chosen after the fourth iteration. With these combinations, solutions converged smoothly to a 1% convergence criterion of the relative velocity within four to five iterations for all steps.

Figure 2 shows the resulting streamline contours for various Reynolds numbers. The influence of STU is also shown at each Reynolds number. Values of the streamline contours are shown in Table I. Results without STU are generally comparable to those of Ghia *et al.*[15] STU contributes to the damping of the peaks of stream function values at the centre of vortices, particularly in high-Reynolds-number cases. The basic idea of STU in FIDAP has its origin in the balancing tensor

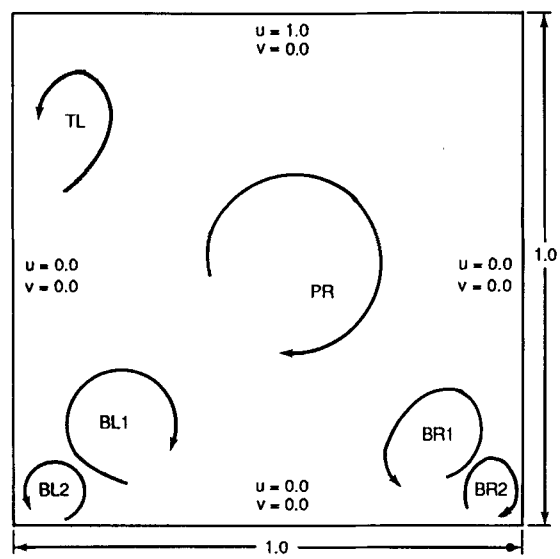

Figure 1. Geometry and boundary conditions of 2D laminar flow inside a wall-driven cavity

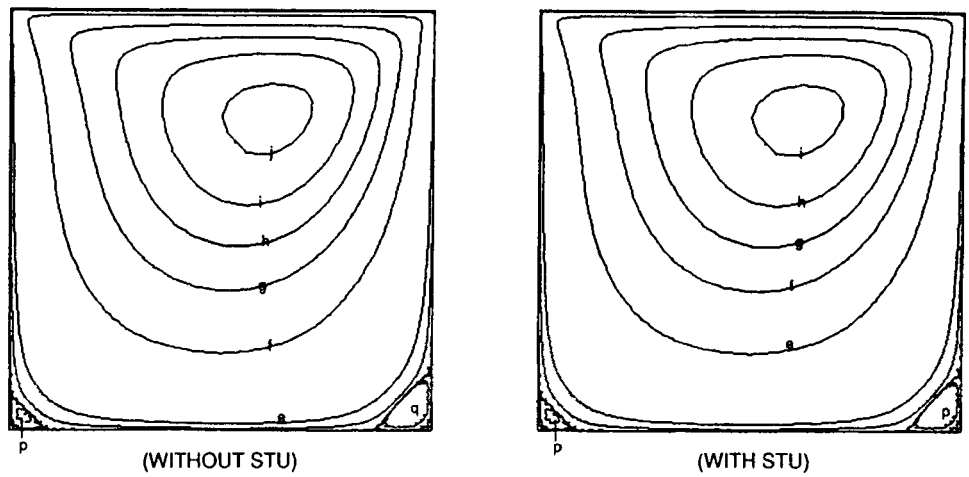

(a) Re = 100

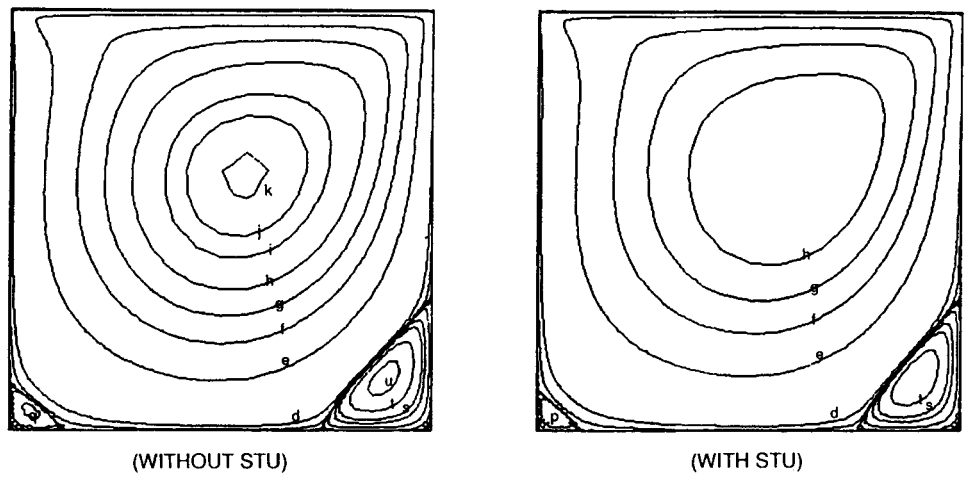

(b) Re = 400

Figure 2. Streamline contours of 2D laminar flow inside a wall-driven cavity

diffusivity (BTD) of Gresho *et al.*,[13] which was proposed to improve accuracy and stability in the forward Euler time integration of the transient case. The basic concept of BTD and its relationship to STU in the steady state is reviewed in the Appendix. The diffusive behaviour of solutions with STU may be related to the following factors: (1) the choice of upwind constant, which is controllable by users, may be inappropriate, and (2) the third-order differential term in equation (13) in the Appendix may not be negligibly small, especially when a C^0-continuous quadratic interpolation function is used for velocity in the region of relatively small local Reynolds numbers.

Pressure contours are shown in Figure 3 and their values given in Table I. STU reduces the total pressure differences ($\Delta P = P_{max} - P_{min}$) for all Reynolds numbers. Comparing these results with the results of Gresho *et al.*[16] for $Re = 5000$ and 10000, the ΔP of the present study without STU

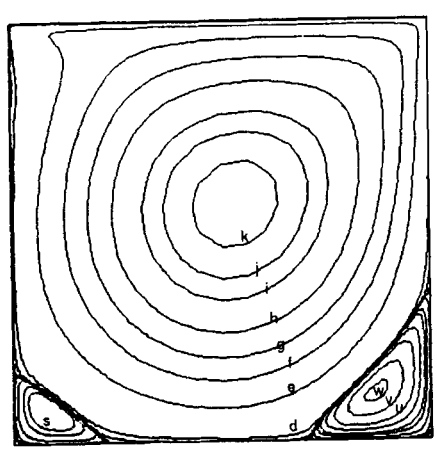

(WITHOUT STU)

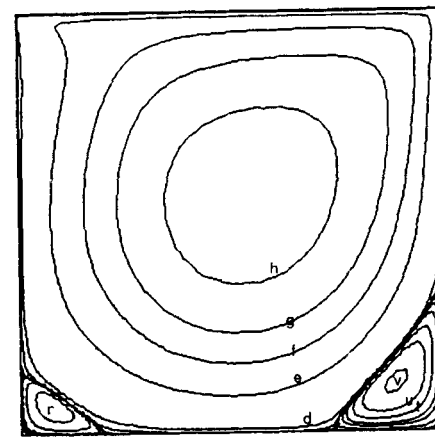

(WITH STU)

(c) Re = 1000

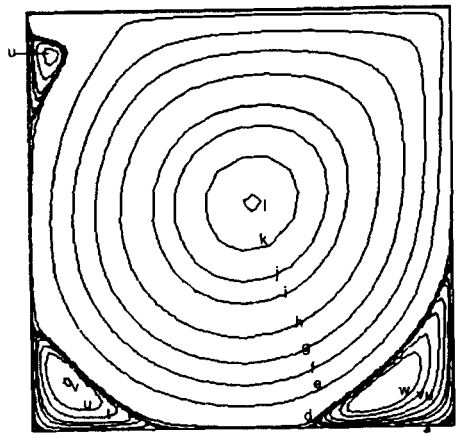

(WITHOUT STU)

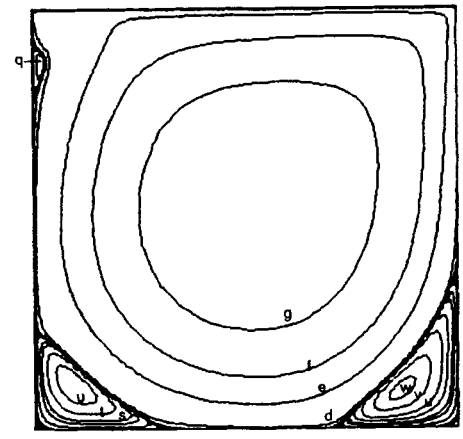

(WITH STU)

(d) Re = 3200

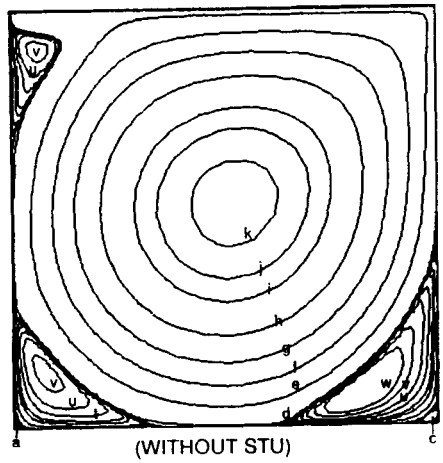

(WITHOUT STU)

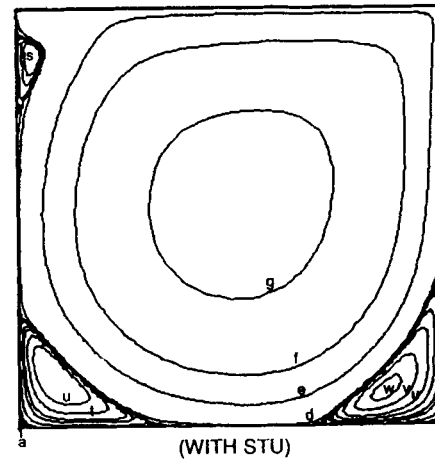

(WITH STU)

(e) Re = 5000

Figure 2. (Continued)

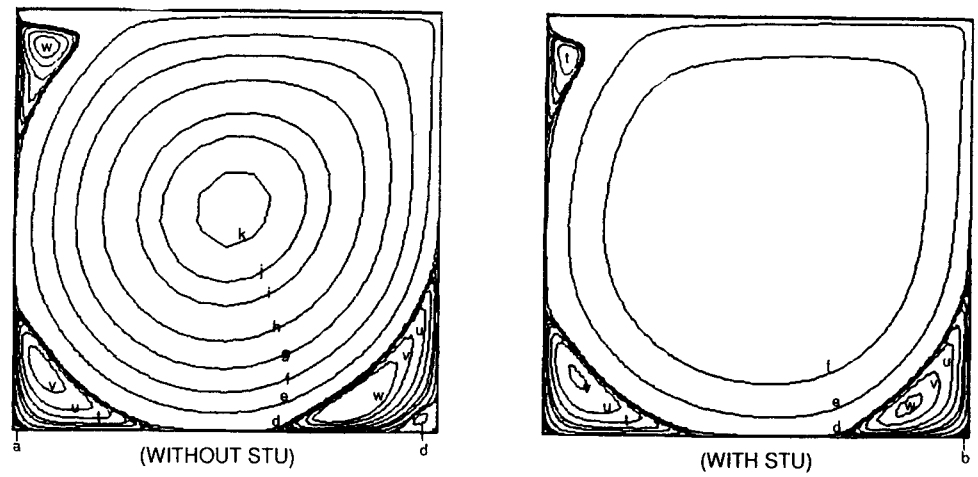

(f) Re = 7500

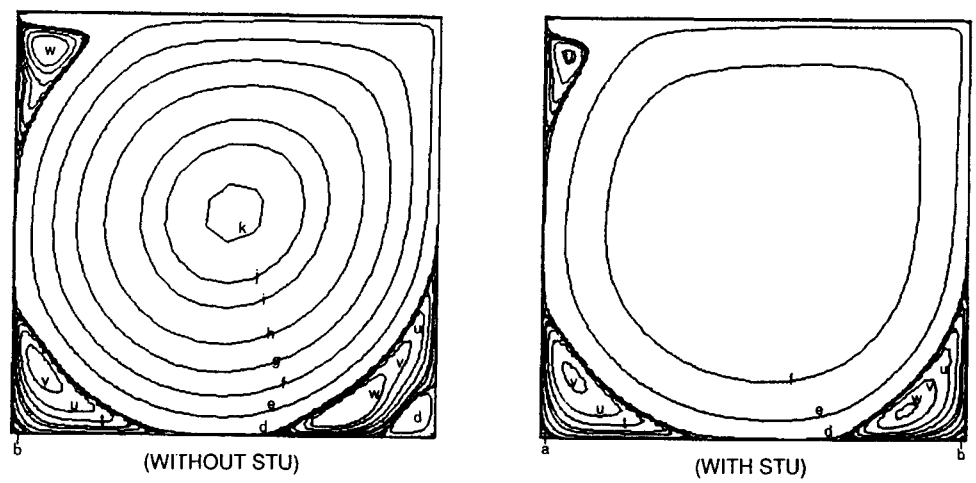

(g) Re = 10,000

Figure 2. (Continued)

are larger than those obtained by Gresho *et al.*, but similar trends for the pressure contours are generated in both cases.

Horizontal velocities along the vertical centreline inside a cavity are compared with the results of Ghia *et al.*[15] in Figure 4. In the case without STU, velocity profiles for all Reynolds numbers are in excellent agreement with those of Ghia *et al.* The minimum difference in the peak velocity is 1·00% at $Re = 100$ and the maximum is 1·57% at $Re = 10000$. On the other hand, when STU is selected, the minimum difference is 8·241% at $Re = 100$ and the maximum is 26·10% at $Re = 10000$. Again, no horizontal components of velocities are generated near the centres in high-Reynolds-number cases when STU is used.

Extreme values of the stream functions for various vortices inside a cavity are shown in Table II. Results of the present study (both with and without STU) are consistently lower than those of

Table I. Values of streamline and pressure contours in Figures 2 and 3

Label	Streamline	Pressure
a	$-1{\cdot}0 \times 10^{-10}$	−0·1000
b	$-1{\cdot}0 \times 10^{-7}$	−0·0900
c	$-1{\cdot}0 \times 10^{-5}$	−0·0800
d	$-1{\cdot}0 \times 10^{-4}$	−0·0700
e	−0·0100	−0·0600
f	−0·0300	−0·0500
g	−0·0500	−0·0400
h	−0·0700	−0·0300
i	−0·0900	−0·0200
j	−0·1000	−0·0100
k	−0·1100	0·0000
l	−0·1150	0·0100
m	−0·1175	0·0200
n	$1{\cdot}0 \times 10^{-8}$	0·0300
o	$1{\cdot}0 \times 10^{-7}$	0·0400
p	$1{\cdot}0 \times 10^{-6}$	0·0500
q	$1{\cdot}0 \times 10^{-5}$	0·0600
r	$5{\cdot}0 \times 10^{-5}$	0·0700
s	$1{\cdot}0 \times 10^{-4}$	0·0800
t	$2{\cdot}5 \times 10^{-4}$	0·0900
u	$5{\cdot}0 \times 10^{-4}$	0·1000
v	$1{\cdot}0 \times 10^{-3}$	—
w	$1{\cdot}5 \times 10^{-3}$	—
x	$3{\cdot}0 \times 10^{-3}$	—

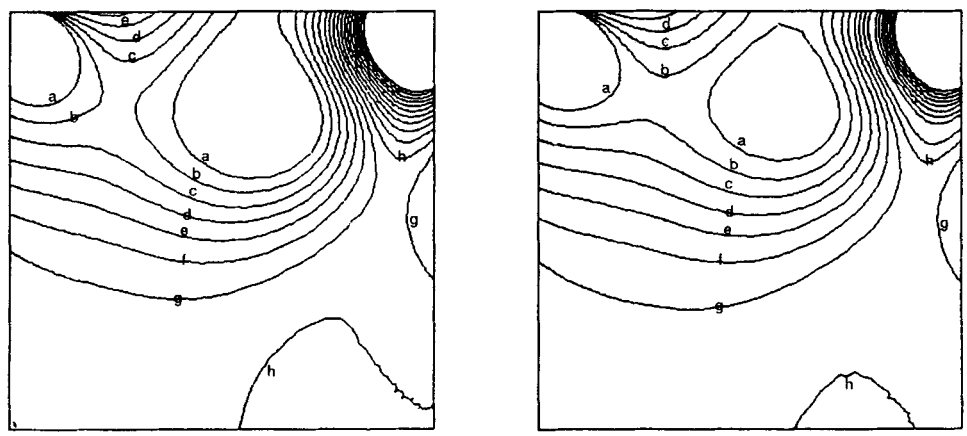

(a) Re = 100

Figure 3. Pressure contours of 2D laminar flow inside a wall-driven cavity

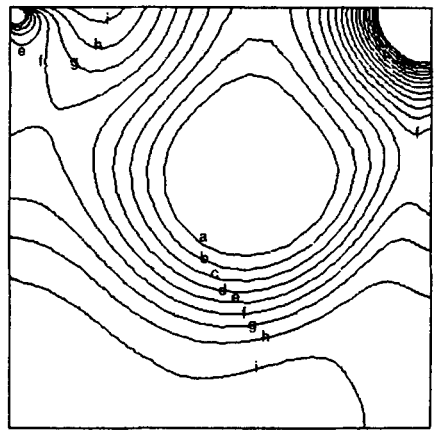

(WITHOUT STU)

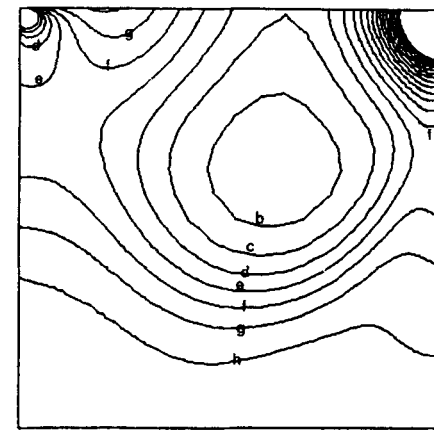

(WITH STU)

(b) Re = 400

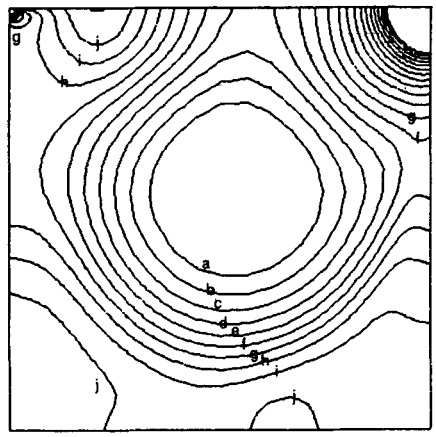

(WITHOUT STU)

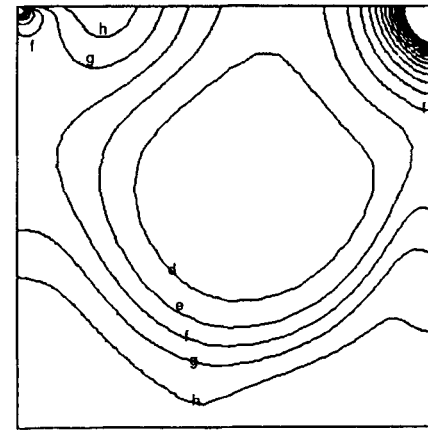

(WITH STU)

(c) Re = 1000

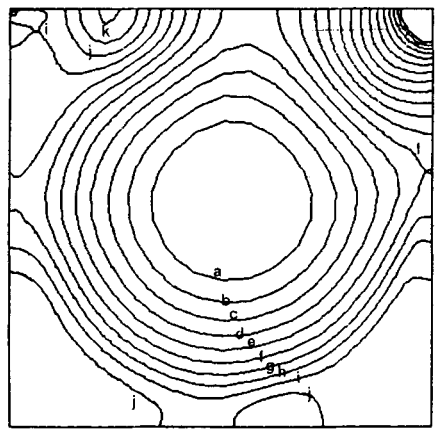

(WITHOUT STU)

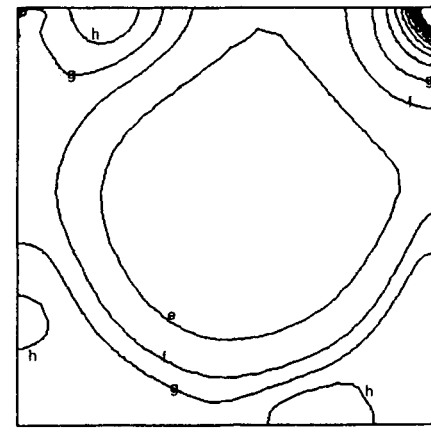

(WITH STU)

(d) Re = 3200

Figure 3 (Continued)

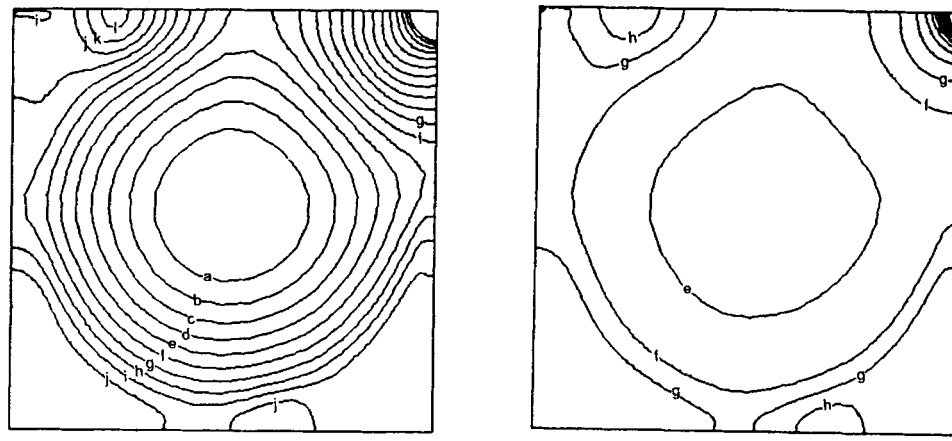

(WITHOUT STU) (WITH STU)

(e) Re = 5000

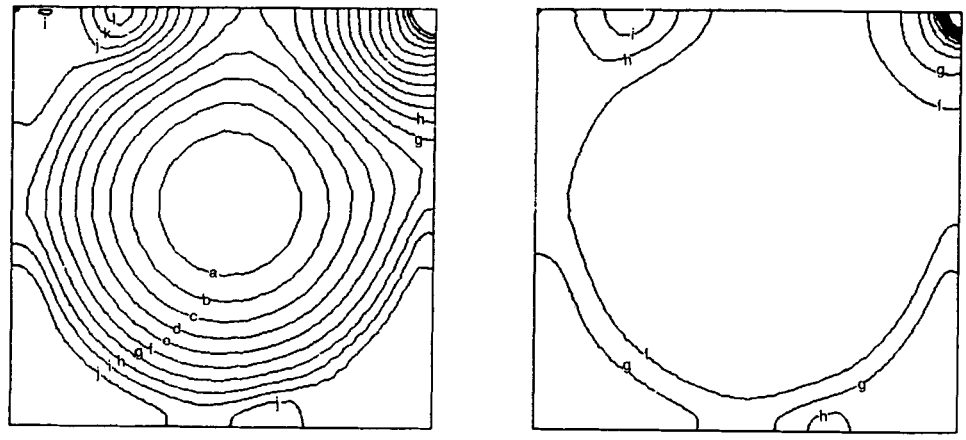

(WITHOUT STU) (WITH STU)

(f) Re = 7500

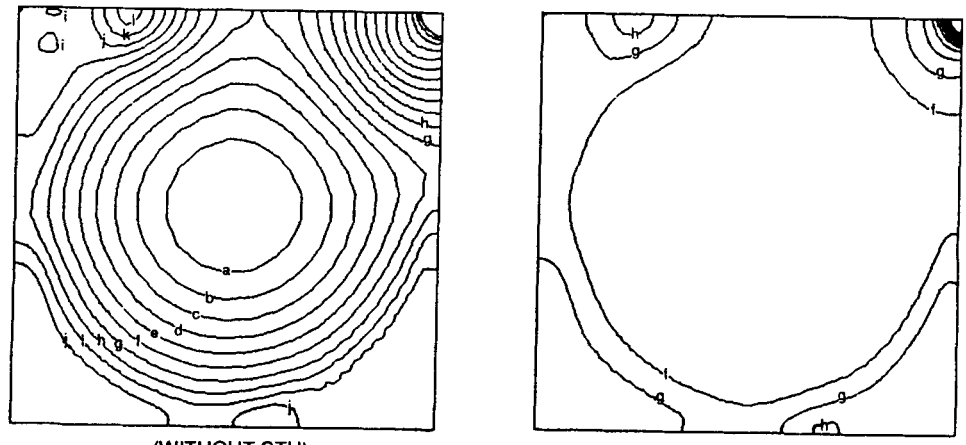

(WITHOUT STU) (WITH STU)

(g) Re = 10,000

Figure 3 (Continued)

Table II. Extreme values of stream functions at various vortices inside a wall-driven cavity

Vortex	Case	Reynolds number						
		100	400	1000	3200	5000	7500	10,000
PR (primary vortex)	Present study without STU	−0·102356	−0·111768	−0·115095	−0·115658	−0·114762	−0·113321	−0·112070
	Present study with STU	−0·095996	−0·090032	−0·079853	−0·061537	−0·054081	−0·047444	−0·042915
	Ghia *et al.*	−0·103423	−0·113909	−0·117929	−0·120377	−0·118966	−0·119976	−0·119731
	Gresho *et al.*			−0·114	−0·118	−0·109	−0·108	−0·101
TL (top left)	Present study without STU	—	—	—	$6{\cdot}0639 \times 10^{-4}$	$1{\cdot}2833 \times 10^{-3}$	$1{\cdot}8255 \times 10^{-3}$	$2{\cdot}1824 \times 10^{-3}$
	Present study with STU	—	—	—	$2{\cdot}3392 \times 10^{-5}$	$1{\cdot}9489 \times 10^{-4}$	$4{\cdot}3026 \times 10^{-4}$	$5{\cdot}4642 \times 10^{-4}$
	Ghia *et al.*	—	—	—	$7{\cdot}2768 \times 10^{-4}$	$1{\cdot}4564 \times 10^{-3}$	$2{\cdot}0462 \times 10^{-3}$	$2{\cdot}4210 \times 10^{-3}$
	Gresho *et al.*			—	$5{\cdot}86 \times 10^{-4}$	$1{\cdot}23 \times 10^{-3}$	$1{\cdot}84 \times 10^{-3}$	$2{\cdot}23 \times 10^{-3}$
BL1 (secondary bottom left)	Present study without STU	$1{\cdot}6913 \times 10^{-6}$	$1{\cdot}3244 \times 10^{-5}$	$2{\cdot}1730 \times 10^{-4}$	$1{\cdot}0447 \times 10^{-3}$	$1{\cdot}2533 \times 10^{-3}$	$1{\cdot}5534 \times 10^{-3}$	$1{\cdot}3732 \times 10^{-3}$
	Present study with STU	$1{\cdot}5288 \times 10^{-6}$	$5{\cdot}9496 \times 10^{-6}$	$9{\cdot}4107 \times 10^{-5}$	$7{\cdot}1664 \times 10^{-4}$	$9{\cdot}4147 \times 10^{-4}$	$1{\cdot}0875 \times 10^{-3}$	$1{\cdot}1390 \times 10^{-3}$
	Ghia *et al.*		$1{\cdot}4195 \times 10^{-5}$	$2{\cdot}3113 \times 10^{-4}$	$9{\cdot}7823 \times 10^{-4}$	$1{\cdot}3612 \times 10^{-3}$	$1{\cdot}4671 \times 10^{-3}$	$1{\cdot}5183 \times 10^{-3}$
	Gresho *et al.*	$1{\cdot}7488 \times 10^{-6}$		$2{\cdot}0 \times 10^{-4}$	$1{\cdot}2 \times 10^{-3}$	$1{\cdot}49 \times 10^{-3}$	$1{\cdot}75 \times 10^{-3}$	$1{\cdot}93 \times 10^{-3}$
BL2 (tertiary bottom left)	Present study without STU	—	—	—	$-3{\cdot}4498 \times 10^{-8}$	$-4{\cdot}9318 \times 10^{-8}$	$-1{\cdot}0236 \times 10^{-7}$	$-4{\cdot}0672 \times 10^{-7}$
	Present study with STU	—	—	—	$-2{\cdot}2516 \times 10^{-8}$	$-3{\cdot}5332 \times 10^{-8}$	$-4{\cdot}5713 \times 10^{-8}$	$-9{\cdot}5564 \times 10^{-8}$
	Ghia *et al.*	—	$-7{\cdot}6774 \times 10^{-10}$	—	$-6{\cdot}3300 \times 10^{-8}$	$-7{\cdot}0886 \times 10^{-8}$	$-1{\cdot}8317 \times 10^{-7}$	$-7{\cdot}7565 \times 10^{-7}$
	Gresho *et al.*			$-1{\cdot}14 \times 10^{-9}$	$-1{\cdot}0 \times 10^{-8}$	$-2{\cdot}85 \times 10^{-8}$	$-2{\cdot}74 \times 10^{-7}$	$-3{\cdot}08 \times 10^{-8}$
BR1 (secondary bottom right)	Present study without STU	$1{\cdot}1605 \times 10^{-5}$	$6{\cdot}1254 \times 10^{-4}$	$1{\cdot}6267 \times 10^{-3}$	$2{\cdot}6022 \times 10^{-3}$	$2{\cdot}8014 \times 10^{-3}$	$2{\cdot}8585 \times 10^{-3}$	$2{\cdot}7994 \times 10^{-3}$
	Present study with STU	$9{\cdot}3406 \times 10^{-6}$	$4{\cdot}2017 \times 10^{-4}$	$1{\cdot}1015 \times 10^{-3}$	$1{\cdot}6599 \times 10^{-3}$	$1{\cdot}7164 \times 10^{-3}$	$1{\cdot}6665 \times 10^{-3}$	$1{\cdot}5897 \times 10^{-3}$
	Ghia *et al.*	$1{\cdot}2537 \times 10^{-5}$	$6{\cdot}4235 \times 10^{-4}$	$1{\cdot}7501 \times 10^{-3}$	$3{\cdot}1396 \times 10^{-3}$	$3{\cdot}0836 \times 10^{-3}$	$3{\cdot}2848 \times 10^{-3}$	$3{\cdot}4183 \times 10^{-3}$
	Gresho *et al.*			$1{\cdot}76 \times 10^{-3}$	$3{\cdot}29 \times 10^{-3}$	$3{\cdot}87 \times 10^{-3}$	$4{\cdot}86 \times 10^{-3}$	$5{\cdot}54 \times 10^{-3}$
BR2 (tertiary bottom right)	Present study without STU	—	$-1{\cdot}6324 \times 10^{-8}$	$-1{\cdot}2032 \times 10^{-8}$	$-1{\cdot}2434 \times 10^{-7}$	$-7{\cdot}1179 \times 10^{-7}$	$-1{\cdot}4305 \times 10^{-5}$	$-6{\cdot}8072 \times 10^{-5}$
	Present study with STU	—	$-1{\cdot}1556 \times 10^{-8}$	$-1{\cdot}4968 \times 10^{-8}$	$-5{\cdot}5793 \times 10^{-8}$	$-7{\cdot}0963 \times 10^{-8}$	$-1{\cdot}5882 \times 10^{-7}$	$-5{\cdot}2657 \times 10^{-7}$
	Ghia *et al.*	—	$-1{\cdot}8659 \times 10^{-8}$	$-9{\cdot}3193 \times 10^{-8}$	$-2{\cdot}5165 \times 10^{-7}$	$-1{\cdot}4322 \times 10^{-6}$	$-3{\cdot}2815 \times 10^{-5}$	$-1{\cdot}3132 \times 10^{-4}$
	Gresho *et al.*			$-1{\cdot}8 \times 10^{-8}$	$-2{\cdot}05 \times 10^{-7}$	$-5{\cdot}22 \times 10^{-8}$	$-7{\cdot}46 \times 10^{-5}$	$-2{\cdot}02 \times 10^{-4}$

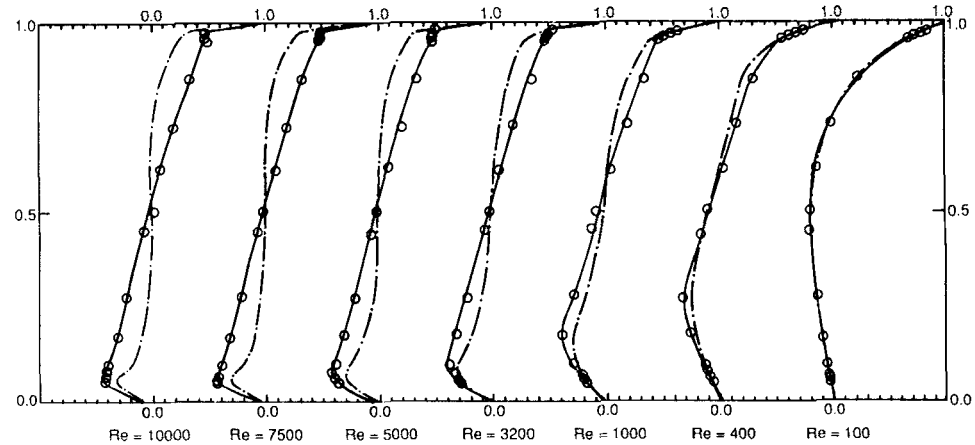

Figure 4. Comparison of u-velocities along a vertical centreline:——, present study without STU; ——·——, present study with STU; ○, Ghia *et al.*

Ghia *et al.*[15] for all Reynolds numbers. When STU is not used, the differences from the results of Ghia *et al.* are 1·03% to 6·40% for the primary vortex, 3·28% to 18·1% for the bottom vortices and 9·85% to 16·67% for the top left vortex. The extreme values of the stream functions for the primary vortex are higher than those of Gresho *et al.*[16] This may be simply due to the finer grid ($h = 0{\cdot}03074$) employed in the central region compared to that in Gresho *et al.* ($h = 0{\cdot}060$).

2D laminar flow over a backward-facing step

The geometry and boundary conditions are shown in Figure 5. The aspect ratio of the backward-facing step (h) to the overall cross-sectional width is 1:2, and the total length in the horizontal direction is 30 h. A fully developed parabolic velocity profile is prescribed at the inlet boundary. Predicted results are compared with experimental measurements of Armaly *et al.*[17]

30 × 16 elements (61 × 33 grid points) are used with fine meshes near the walls and in the mixing zone along the centreline. Selected Reynolds numbers are 100, 200, 300, 400, 500, 600, 700 and 800. Here, the Reynolds number is based on the bulk velocity at the inlet boundary and the cross-sectional width of the whole domain as defined in Armaly *et al.*[17] The same restart procedure as in the previous case is adopted. Also, the combination of the successive substitution and quasi-Newton methods is used for the non-linear solutions. Four to five iterations were performed in each step for 1% convergence of relative velocity.

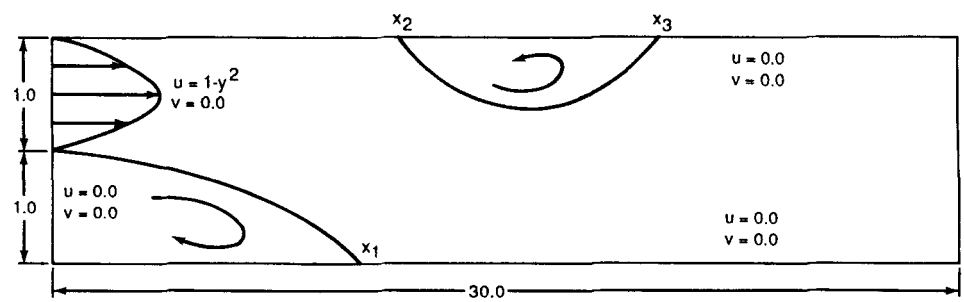

Figure 5. Geometry and boundary conditions of 2D laminar flow over a backward-facing step

Figure 6 represents streamline contours for selected Reynolds numbers. Values of the contours are given in Table III. The recirculating zone behind a backward-facing step becomes larger as the Reynolds number increases, and another recirculating zone near the upper wall is generated after $Re = 500$. STU reduces peak streamline levels of both recirculating zones. Pressure contours are shown in Figure 7 and Table III for selected Reynolds numbers. As the Reynolds number increases, the order of magnitude of the pressure becomes smaller and the position of maximum pressure moves downstream. At a fixed Reynolds number the total pressure difference in the case with STU is larger than in that without STU.

Comparisons with experimental data of Armaly *et al.*[17] are shown in Figure 8. There is excellent agreement between predicted reattachment lengths and experimental measurements. Discrepancies between computational predictions and experimental data at high Reynolds numbers may come from three-dimensional effects of the experiments. The general trend of the curve of x_1 (the reattachment length of the recirculating zone behind a backward-facing step) is the same as that of Kim and Moin[18] who used the finite difference method with 101×101 grid points. Also, predictions of beginning (x_2) and end (x_3) points of the recirculating zone near the upper wall compare satisfactorily with experimental data. With STU, x_1 becomes longer by 1·3% ($Re = 800$) to 8·0% ($Re = 100$) and x_2 and x_3 are shifted downstream at low Reynolds number, upstream at high Reynolds number. The width of the recirculating zone near the upper wall is decreased by a maximum of 34·4% at $Re = 500$ and by a minimum of 2·7% at $Re = 800$ by STU.

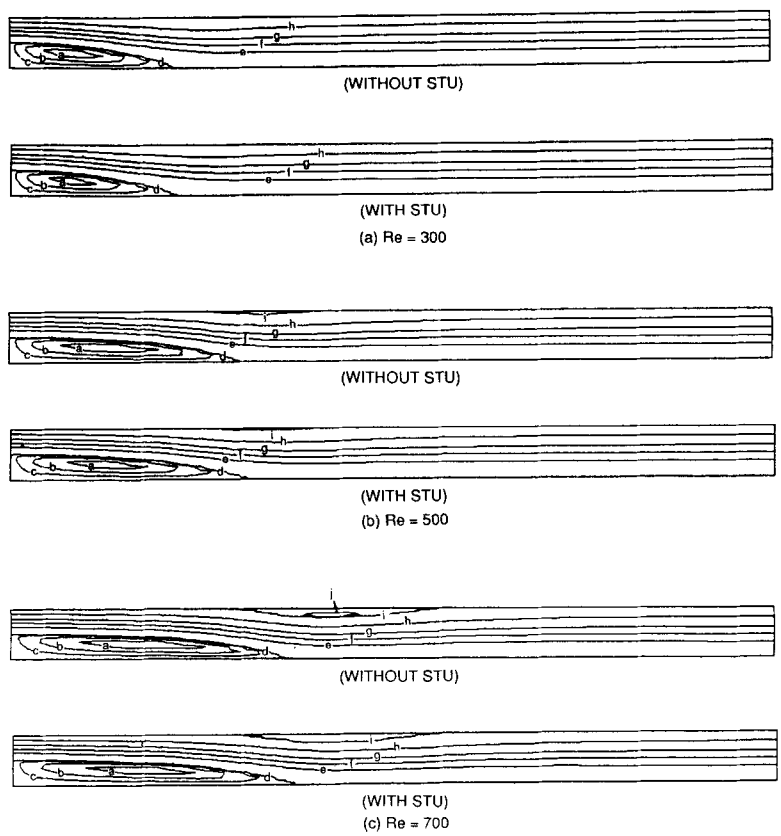

Figure 6. Streamline contours of 2D laminar flow over a backward-facing step

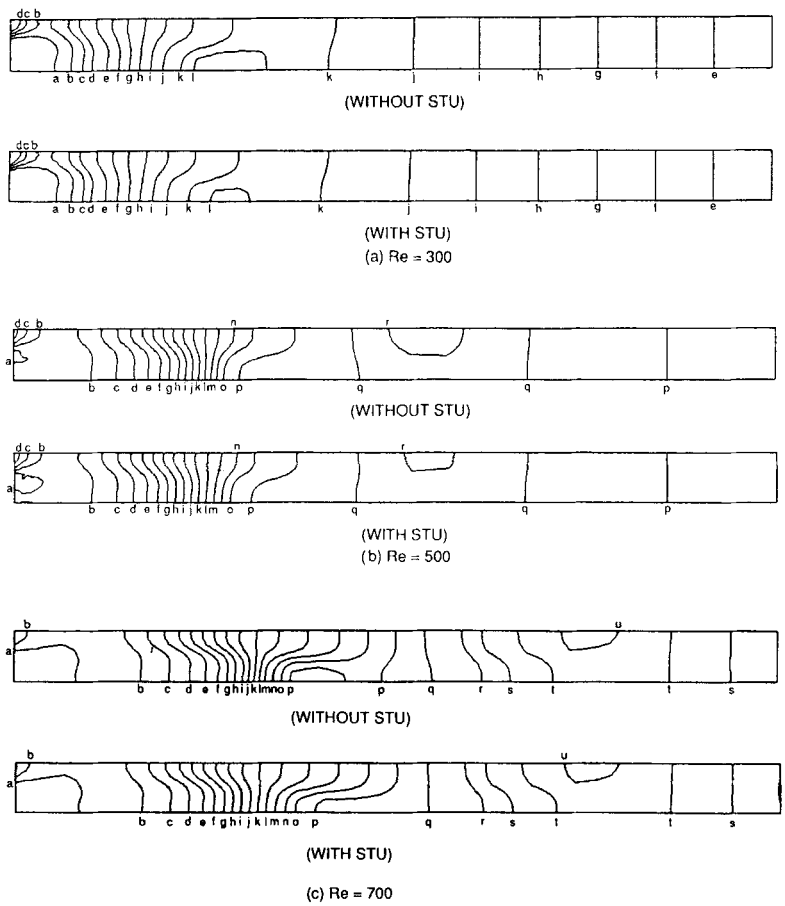

Figure 7. Pressure contours of 2D laminar flow over a backward-facing step

2D turbulent flow over a backward-facing step

The last test case is one of the standard test cases of complex turbulent flows presented at the 1980–1981 Stanford Conference.[19] The geometry and boundary conditions are shown in Figure 9. The aspect ratio of the backward-facing step (h) to the overall cross-sectional width is 1:3, and the total length in the horizontal direction behind a backward-facing step is $24h$. As previously mentioned, the standard k–ε turbulence model of Launder and Spalding[14] is used with wall functions on non-slip walls. Uniform velocity is given along the inlet boundary. Inlet boundary conditions for k and ε are prescribed as follows:

$$k = 0{\cdot}003\, u_0^2, \qquad \varepsilon = C_\mu k^{1{\cdot}5} l^{-1},$$

where $l = 0{\cdot}03\, h$.

The Reynolds number, based on the inlet velocity and the height of a backward-facing step, is chosen as 69610, which represents the same flow conditions as Kim *et al.*[20] 22×16 nine-node quadrilateral elements (45×33 grid points) are used with fine meshes near the walls. For the iterative solutions of the non-linear equations the successive substitution method (acceleration factor = 0·5) was used. When STU was used, the solution converged to a 0·001% convergence

Table III. Values of streamline and pressure contours in Figures 6 and 7

Label	Streamline	Pressure		
		$Re=300$	$Re=500$	$Re=700$
a	−0·0250	−0·0075	−0·0350	−0·1431
b	−0·0150	−0·0050	−0·0325	−0·0400
c	−0·0050	−0·0025	−0·0300	−0·0375
d	0·0000	−0·0000	−0·0275	−0·0350
e	0·1000	−0·0050	−0·0250	−0·0325
f	0·2000	−0·0100	−0·0225	−0·0300
g	0·3000	−0·0150	−0·0200	−0·0275
h	0·4000	−0·0200	−0·0175	−0·0250
i	0·4391	−0·0250	−0·0150	−0·0225
j	0·4408	−0·0300	−0·0125	−0·0200
k	—	0·0350	0·0100	0·0175
l	—	0·0370	0·0075	0·0150
m	—	—	0·0050	0·0125
n	—	—	0·0025	0·0100
o	—	—	0·0000	0·0075
p	—	—	0·0050	0·0050
q	—	—	0·0100	0·0025
r	—	—	0·0115	0·0000
s	—	—	—	0·0010
t	—	—	—	0·0020
u	—	—	—	0·0025

criterion of the relative velocity with 65 iterations. Newton-type iterative methods were not suitable for this particular problem because of complex non-linear terms in the turbulence transport equations. When STU was not selected, undershootings (negative values) in the solutions of the turbulent transport equations appeared after four to five iterations, and solutions started to diverge.

Figure 10 represents streamline contours. The most important parameter for comparison with the experimental data of Kim *et al.*[20] is the reattachment length X_r of the separation zone behind a backward-facing step. The acceptable experimental measurement of X_r is $7{\cdot}0 \pm 1{\cdot}0$.[20] The predicted value in the present study is 5·59, which is comparable to the finite difference results of 5·2 to 5·8 reported at the 1980–1981 Stanford Conference.[19] Underpredictions of X_r can be explained as follows: (1) the k–ε turbulence model may be inappropriate to model recirculating turbulent flows, and (2) numerical diffusion of upwinding schemes may influence the velocity distribution. For example, Heckman *et al.*[21] predicted X_r as 6·5 using the skew hybrid upstream finite differencing scheme for the momentum equations and the upstream weighted finite differencing scheme for the turbulent transport equations. More recently, Betts and Haroutunian[22] reported X_r as 6·23 using the explicit time-marching finite element method with BTD, but their computations required special treatments for the k and ε equations to prevent undershootings due to the higher-order accuracy of the BTD scheme. In both Hackman *et al.*[21] and Betts and Haroutunian[22] the longer predictions of X_r resulted from higher-order upwinding schemes for the momentum equations, but those schemes cannot be used for the turbulent transport equations. The influence of STU on X_r in the present study can also be explained by the same factors mentioned in the first example. However, STU is essential to obtain converged solutions in this particular case.

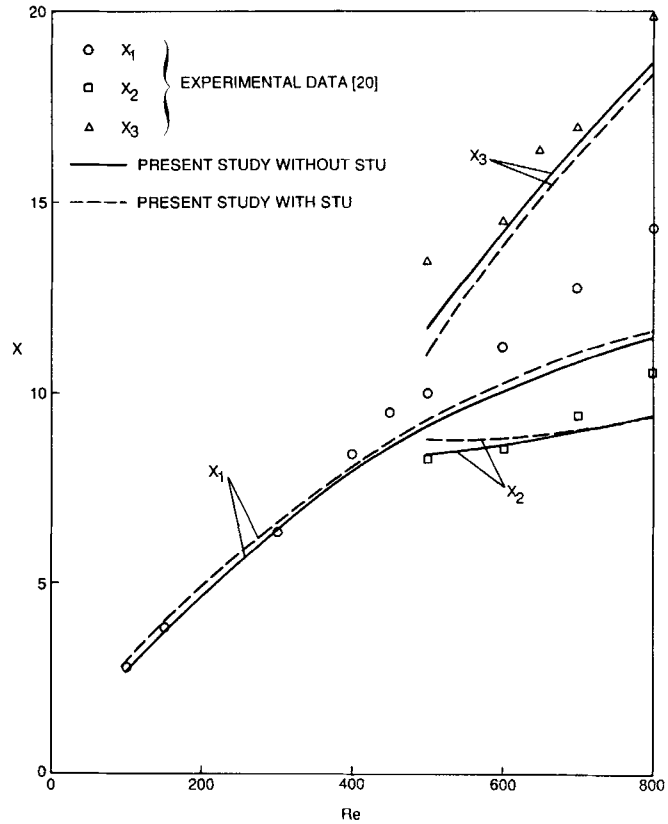

Figure 8. Comparison of reattachment lengths of 2D laminar flow over a backward-facing step

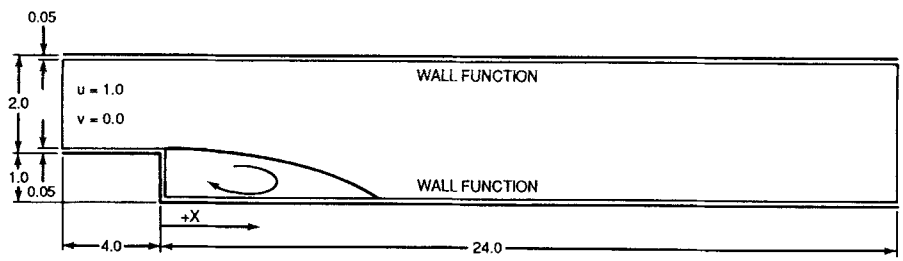

Figure 9. Geometry and boundary conditions of 2D turbulent flow over a backward-facing step

Figure 10. Streamline contours of 2D turbulent flow over a backward-facing step

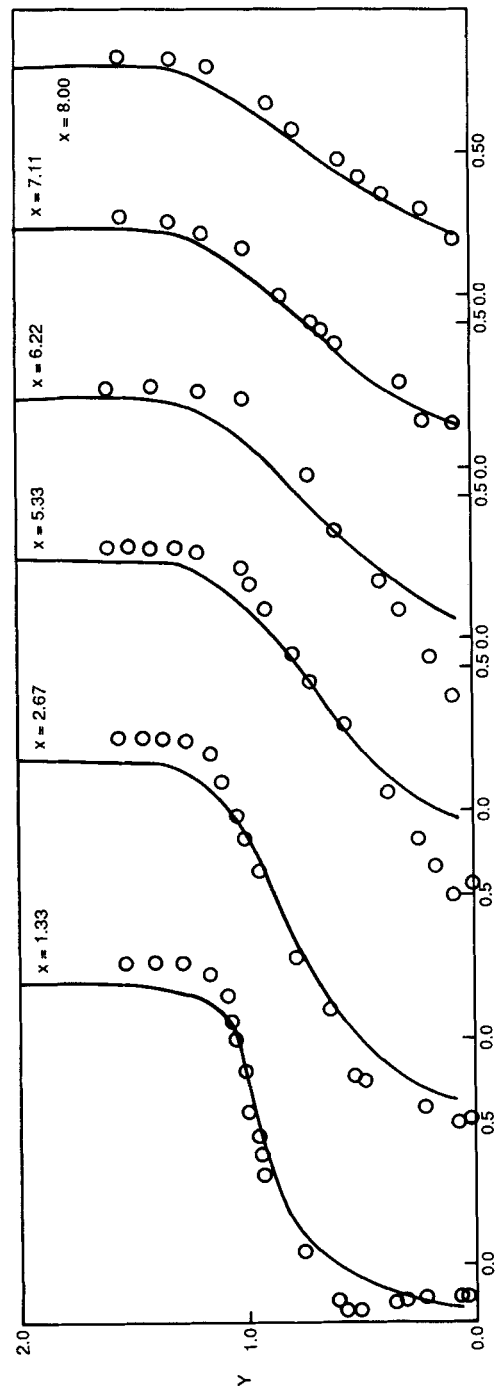

Figure 11. Comparison of predicted and measured velocities for 2D turbulent flow over a backward-facing step: —— present study; ○, experimental data of Kim *et al.*

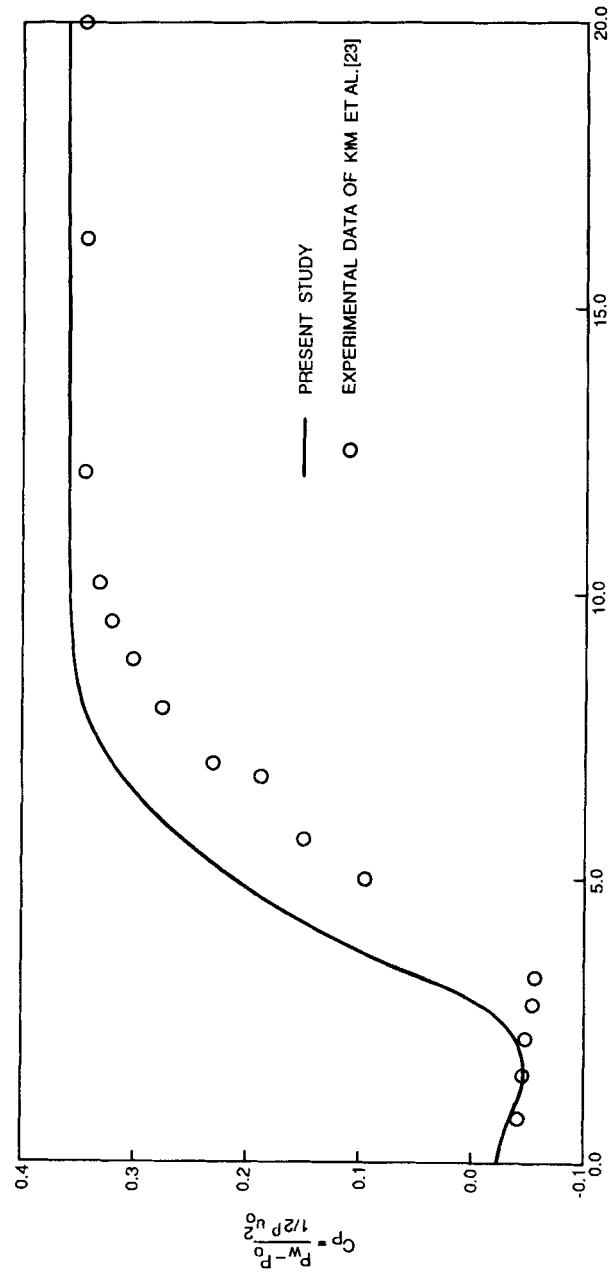

Figure 12. Comparison of predicted and measured pressure coefficient for 2D turbulent flow over a backward-facing step

Figure 13. Contours of turbulent kinetic energy of 2D turbulent flow over a backward-facing step

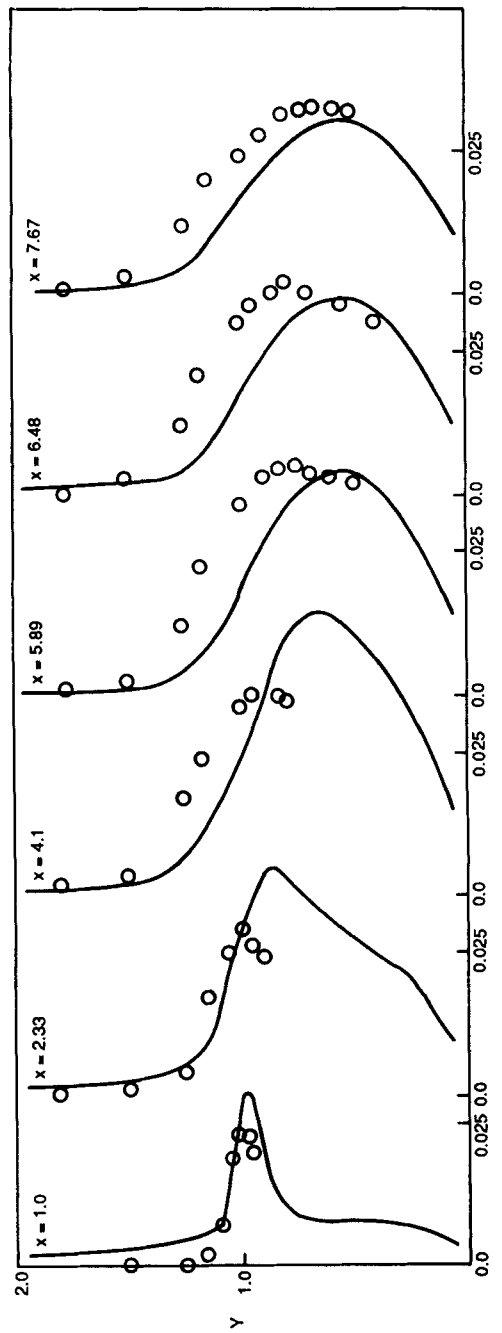

Figure 14. Comparison of predicted and measured turbulent kinetic energy for 2D, turbulent flow over a backward-facing step: ——, present study; ○, experimental data of Kim *et al.*

Table IV. Values of streamline and turbulent kinetic energy contours in Figures 10 and 11

Label	Streamline	Turbulent kinetic energy
a	−0·0600	0·0450
b	−0·0400	0·0400
c	−0·0200	0·0350
d	0·0000	0·0300
e	0·2000	0·0250
f	0·4000	0·0200
g	0·6000	0·0150
h	0·8000	0·0100
i	1·0000	—
j	1·2000	—
k	1·4000	—
l	1·6000	—
m	1·8000	—

In Figure 11 the predicted mean velocity profiles are compared with experimental measurements. The predictions agree reasonably with the experimental data in the downstream region, but there are some differences between predictions and measurements in the separation region and near the wall. Figure 12 shows a comparison of the pressure coefficients C_p. In the present study the velocity and pressure at the centre of the inlet boundary are selected as reference velocity and pressure for calculation of the pressure coefficients. C_p is generally predicted quite well except in the separation zone. The predicted value of C_p in the downstream region is 0·36.

Contours of the turbulent kinetic energy (TKE) are shown in Figure 13. The peak TKE values exist at the centre of a separation region, and steep gradients of the TKE exist near the mixing zone and solid walls. Values of streamline and TKE contours are shown in Table IV. Predicted TKE values are compared with experimental data in Figure 14. The location of maximum TKE moves close to the wall in the downstream rigion. Differences between predictions and measurements are apparent near the separation and mixing zones. The overprediction of the TKE in the separation region may be the cause of the underprediction of the reattachment length.

CONCLUSIONS

Some classical benchmark problems in 2D laminar and turbulent incompressible fluid flows have been tested for the evaluation of the numerical accuracy of FIDAP. As a result of the present study, the following conclusions are drawn:

1. The consistent integration penalty finite element method with a Q_2/P_1 finite element is efficient for the treatment of velocity–pressure coupling of incompressible fluid flow.
2. Numerical results of FIDAP on laminar flow cases are in good agreement with other CFD solutions and experimental data when STU is not used.
3. When STU is used (with quadratic interpolation functions for velocity) in laminar flow cases, velocity distributions and corresponding pressures are significantly influenced by STU, especially in the area where local Reynolds numbers are relatively low. [Editorial (PMG) remark: This behaviour is actually not so surprising when it is realized that the 'effective Δt' (see Appendix) of STU is relatively large in regions of low velocity.]

4. STU is useful for obtaining solutions of turbulent flow, but it contributes to underprediction of the reattachment length of a separation zone.

ACNOWLEDGEMENT

This work was supported under Contract NAS8-35918 with the NASA/Marshall Space Flight Center.

APPENDIX

In this Appendix the origin of a balancing tensor diffusivity (BTD) is reviewed using a simple advection–diffusion equation:

$$\frac{\partial T}{\partial t} + U_j \frac{\partial T}{\partial x_j} = K \frac{\partial^2 T}{\partial x_j \partial x_j}. \tag{11}$$

Here, for simplicity, it is assumed that K is a constant, U_j is a function of space only and $\partial U_j / \partial x_j = 0$.

Using a conventional Taylor series expansion, the exact solution T^{n+1} at time $t^{n+1} = t^n + \Delta t$ is expressed by

$$T^{n+1} = T^n + \Delta t \left(\frac{\partial T}{\partial t} \right)^n + \frac{\Delta t^2}{2} \left(\frac{\partial^2 T}{\partial t^2} \right)^n + \dots . \tag{12}$$

Combining with equation (11), equation (12) can be rewritten as

$$\begin{aligned} T^{n+1} = T^n - \Delta t\, U_j \frac{\partial T}{\partial x_j} + \Delta t \left(K + \frac{\Delta t^2}{2} \right) \frac{\partial^2 T^n}{\partial x_j \partial x_j} \\ - \Delta t^2 K U_j \frac{\partial^3 T^n}{\partial x_j \partial x_i \partial x_i} - \frac{\Delta t^2}{2} K^2 \frac{\partial^4 T^n}{\partial x_j \partial x_j \partial x_i \partial x_i} \\ - \dots . \end{aligned} \tag{13}$$

Therefore the forward Euler time integration form of equation (11) has the form

$$\frac{T^{n+1} - T^n}{\Delta t} + U_j \frac{\partial T^n}{\partial x_j} = \left(K + \frac{\Delta t}{2} U_j U_j \right) \frac{\partial^2 T^n}{\partial x_i \partial x_i}, \tag{14}$$

neglecting all terms higher than the second-order differential terms.

The last term in equation (14) is the so-called balancing tensor diffusivity (BTD) term. As mentioned in Gresho *et al.*,[13] equation (14) maintains a second-order accuracy only if $K \Delta t < O(\Delta x^2)$, otherwise the accuracy is lower than second-order.

In the steady state there are no clear definitions for the choice of Δt. For example, in FIDAP[9] Δt is defined as FAC $\times\, h^* / \sqrt{(15)\, U_j U_j}$, where h^* is a measure of the element size and FAC is a factor that may be set by users.

REFERENCES

1. J. T. Oden and L. C. Wellford, 'Analysis of flow of viscous fluids by the finite element method', *AIAA J.*, **10**, 1590–1599 (1972).
2. C. Taylor and P. Hood, 'A numerical solution of the Navier–Stokes equations using the finite element technique', *Comput. Fluids*, **1**, 73–100 (1973).

3. P. Hood and C. Taylor, 'Navier–Stokes equations using mixed interpolation', in J. T. Oden *et al.* (eds), *Finite Element Methods in Flow Problems*, UAH Press, 1974, pp. 121–132.
4. P. S. Huyakorn, C. Taylor, R. L. Lee and P. M. Gresho, 'A comparison of various mixed-interpolation finite elements in the velocity–pressure formulation of the Navier–Stokes equations', *Comput. Fluids*, **6**, 25–35 (1978).
5. R. L. Sani, P. M. Gresho, R. L. Lee and D. F. Griffiths, 'The cause and cure(?) of the spurious pressure generated by certain FEM solutions of the incompressible Navier–Stokes equations: Part 1, *Int. j. numer. methods fluids*, **1**, 17–43 (1981).
6. R. L. Sani, P. M. Gresho, R. L. Lee, D. F. Griffiths and M. Engelman, 'The cause and cure (!) of the spurious pressure generated by certain FEM solutions of the incompressible Navier–Stokes equations: Part 2', *Int. j. numer. methods fluids*, **1**, 171–204 (1981).
7. J. T. Oden and O. P. Jacquotte, 'Stability of some mixed finite element methods for Stokesian flows', *Comput. Methods Appl. Mech. Eng.*, **43**, 231–247 (1984).
8. M. Engelman, R. L. Sani, P. M. Gresho and M. Bercovier, 'Consistent vs. reduced integration penalty methods for incompressible media using several old and new elements', *Int. j. numer. methods fluids*, **2**, 25–42 (1982).
9. *FIDAP Theoretical Manual*, Fluid Dynamics International, Inc., 1986.
10. P. Gresho and R. L. Lee, 'Don't suppress the wiggles—they're telling you something', *Comput. Fluids*, **9**, 223–253 (1981).
11. I. Christie, D. F. Griffiths, A. R. Mitchell and O. C. Zienkiewicz, 'Finite element methods for second order differential equations with significant first derivatives', *Int. j. numer. methods eng.*, **10**, 1389–1396 (1976).
12. A. N. Brooks and T. J. R. Hughes, 'Streamline upwind/Petrov–Galerkin formulations for convection dominated flows with particular emphasis on the incompressible Navier–Stokes equations', *Comput. Methods Appl. Mech. Eng.*, **32**, 199–259 (1982).
13. P. M. Gresho, S. T. Chan, R. L. Lee and G. D. Upson, 'A modified finite element method for solving the time-dependent, incompressible Navier–Stokes equations, Part 1: Theory', *Int. j. numer. methods fluids*, **4**, 557–598 (1984).
14. B. E. Launder and D. B. Spalding, 'The numerical computation of turbulent flows', *Comput. Methods Appl. Mech. Eng.*, **3**, 269–289 (1974).
15. U. Ghia, K. N. Ghia and C. T. Shin, 'High-*Re* solutions for incompressible flow using the Navier–Stokes equations and a multi-grid', *J. Comput. Phys.*, **48**, 387–411 (1982).
16. P. M. Gresho, S. T. Chan, R. L. Lee and C. D. Upson, 'A modified finite element method for solving the time-dependent, incompressible Navier–Stokes equations, Part 2: Applications', *Int. j. numer. methods fluids*, **4**, 619–640 (1984).
17. B. F. Armaly, F. Durst, J. C. F. Pereira and B. Schonung, 'Experimental and theoretical investigation of backward-facing step flow', *J. Fluid Mech.*, **127**, 473–496 (1983).
18. J. Kim and P. Moin, 'Application of a fractional-step method to incompressible Navier–Stokes equations', *J. Comput. Phys.*, **59**, 308–323 (1985).
19. *Proc.* 1980–81 *AFOSR–HTTM–Stanford Conference on Complex Turbulent Flows: Comparison of Computation and Experiment, Vol. I and II*, 1982
20. J. Kim, S. J. Kline and J. P. Johnston, 'Investigation of a reattaching turbulent shear layer: flow over a backward-facing step', *J. Fluid Eng., ASME Trans.*, **102**, 302–308 (1980).
21. L. P. Hackman, G. D. Raithby and A. B. Strong, 'Numerical predictions of flows over backward facing steps', *Int. j. numer. methods fluids*, **4**, 711–724 (1984).
22. P. L. Betts and V. Haroutunian, 'k–ε modelling of turbulent flow over a backward facing step by a finite element method; comparison with finite volume solutions and experiments', in C. Taylor *et al.* (eds), *Proc. 4th Int. Conf. on Numerical Methods in Laminar and Turbulent Flows*, 1985, pp. 574–585.